Damage Evolution and Crack Healing in 2D Vitrimer-based Architected Materials

MS53035 MSE MSc Thesis

Thanos Razis 6149375

Master of Materials Science and Engineering, TU Delft

TU Delft
Delft University of Technology

June 21, 2026

Damage Evolution and Crack Healing in 2D Vitrimer-based Architected Materials

Abstract

Vitrimers have attracted significant attention in recent years as promising alternatives to epoxies and other conventional thermosets. Their dynamic covalent bond-exchange reactions enable healing of cracks and delaminations, as well as reprocessability, all while preserving the underlying crosslinked network. These features are particularly appealing for aerospace materials, where epoxy matrices composites dominate. While numerous recent studies investigate delamination healing in Vitrimer-based composites, far fewer studies have examined their healing performance in architected materials with intricate geometries such as cellular solids. These engineered structures can exhibit mechanical properties unattainable in natural materials, yet their low relative density makes them susceptible to crack initiation and propagation. Integrating Vitrimers into such architectures therefore offers a promising route toward damage tolerant lightweight systems.

This work investigates the healing performance of an adipic acid Vitrimer integrated into two distinct 2D cellular architectures. Specimens were manufactured via waterjet cutting and subjected to cyclic loading to observe crack initiation and propagation throughout the lattice. Subsequent healing cycles were performed using a mold and heat press system to apply the pressure required for crack-face closure and bond-exchange activation. The more compliant architecture accumulated greater damage and was consequently more challenging to heal, whereas the stiffer design recovered its stiffness more readily. Overall, the results demonstrate the feasibility of incorporating Vitrimers and other self-healing polymers into foams and metamaterials, while highlighting the process-design considerations and limitations that must be addressed to achieve reliable mechanical recovery.

Contents

I. Introduction

For many years, the prevailing strategy in materials science focused on engineering materials with high strength and durability to resist externally applied loads and thus prevent damage [1]. However, it later became evident that the incorporation of self-healing capabilities could significantly improve service life and long-term reliability, especially in damage-prone applications [2]. A range of design methodologies have been employed to engineer self-healing polymers, each adapted to address the environmental challenges they are expected to encounter. These materials span a wide spectrum of applications, from self-healing polymers used in ballistics and structural components to polymers tailored for electronics and energy devices [3–5].

Among the established strategies, intrinsic self-healing relies on reversible interaction embedded within the polymer structure [6]. These interactions can be either non-covalent (e.g., hydrogen bonding, metal-ligand coordination, ionic interactions) [7–10] or dynamic covalent, the latter typically being activated by heat [11, 12]. These dynamic interactions introduce reversibility into the polymer network, enabling self-healing, reprocessing, and even recyclability- capabilities that conventional thermosets lack due to their permanent crosslinking. The ability to heal cracks while preserving the stiffness of thermosets is particularly valuable for cellular solids such as foams and mechanical metamaterials. Their low relative density and intricate architecture make them prone to crack formation, which can be mitigated through dynamic covalent bonds that enable self-healing.

II. Theoretical Background

A. Vitrimers & Covalent Adaptable Networks (CANs)

1. Covalent Adaptive Networks (CANs)

For many decades, the reversibility of covalent crosslinks in polymeric materials has remained a great challenge for researchers that would enable them to synthesize self healing thermosets with mechanical properties comparable to those of conventional thermosets. Although dynamic covalent bonds have attracted significant attention in the past decade, the concept of dynamic covalent chemistry was first introduced in the 1950s [13]. Tobolsky (1956) described the chemical reactions that occur in elongated polyurethanes and vulcanized rubber at high temperatures, using the term “chemorheology” [14]. At the time, the concept was regarded theoretically intriguing but without practical applications. However, in recent years, materials scientists have revisited this field and, with the aid of more advanced techniques, have established the foundation of Covalent Adaptable Networks (CANs). Covalent Adaptable Networks are dynamic polymer

materials which are made by a highly cross-linked network where the covalent links between the molecular chains can be dynamically exchanged by a chemical reaction [15–17].

Due to the reversibility of covalent bonds, Covalent Adaptable Networks can permanently reconfigure their topology in response to external triggers (such as pH, heat or light) without causing irreversible degradation of the network structure, thus maintaining their initial bond density [18]. As adaptive polymeric materials, CANs have fundamentally changed the traditional understanding of polymer science. Rather than viewing thermoplastics and thermosets as rigidly distinct categories, there is a continuum between them [19]. CANs can combine the advantages of thermosets, such as structural integrity and mechanical strength, with functionalities such as self-healing, shape transformation under applied stimuli, and recyclability-reprocessability.

The extraordinary properties of CANs arise from their underlying exchange reactions. The crosslink bonds can break and reform to enable healing in a way that allows the network to retain the characteristic crosslinked structure and mechanical properties of a thermoset. Based on the chemical nature of bond exchange reactions, covalent adaptable networks can be categorized into two major groups [15–20] :

- Dissociative: In dissociative CANs, reversible covalent bonds first break and subsequently reattach at a different site of molecular chains, and as a result the reaction occurs in two distinct stages. The first stage causes a temporary reduction in the crosslink density, leading to a decrease in the viscosity and a loss of dimensional integrity so that the network flows. During the second stage, the crosslink density is restored, forcing the material to regain a crosslinked structure. For this class of CANs, the dominant design parameter is the functional group chemistry rather than the use of catalysts, which are sometimes even unnecessary. The thermodynamics of the selected reaction determines the flow, relaxation, and healing behavior of the material.
- Associative: In associative CANs, a new covalent bond forms before the original breaks. Consequently, the cross-link density remains constant and the network maintains its mechanical and dimensional integrity. In this case, the rheological properties depend on the kinetics of the reaction, making catalyst selection a critical factor.

It should be noted that although dynamic bond reactions in CANs can be triggered by a variety of external stimuli, most studies focus on thermally activated systems, or thermoreversible CANs [21]. Several factors contribute to this trend. Heat is the most accessible and universally applicable stimulus, available both in laboratories and in industrial settings. Furthermore, thermal processing has long been the foundation for materials manufacturing for both polymers and metals. Thereby, the most widely used reversible crosslinking reactions in CANs are those that are thermally activated, such as Diels-Alder, Disulfides and Transesterification [15].

Selecting among the two major categories of reversible covalent reactions is a fundamental step in designing and synthesizing a covalent adaptable network because it determines whether the network behaves as associative or dissociative with different dynamics of topology rearrangement and stress relaxation behavior. Dissociative CANs, like thermoplastics, transition from solid to liquid abruptly, following the Williams-Landel-Ferry model [22, 23]. Their sharp decrease in viscosity and consequently in creep resistance makes their mechanical performance less predictable. In contrast, associative CANs can facilitate bond exchange reactions more gradually and controllably. For this reason, assocative CANs and more specifically Vitrimers are more extensively studied for load-bearing applications.

2. Vitrimers

A major landmark in the field of dynamic covalent chemistry came in 2011, when Professor Leibler and his research group introduced transesterification reactions into cross-linked epoxy resin networks [24]. To accelerate the kinetics of the associative reaction, zinc acetate $Zn(ac)_2$ was incorporated as a catalyst. The resulting material behaves like a conventional hard epoxy resin at room temperature, exhibiting a glass transition temperature of 80°C and a modulus of 1.8 GPa. Even at high temperatures, the polymeric material did not dissolve in good solvents over long periods, reflecting once again the typical thermoset behavior. Nevertheless, it can relax stress and flow at elevated temperatures.

Similarly to vitreous silica (SiO_2), the viscosity of these networks follows the Arrhenius equation. For this reason, Leibler and his colleagues named these associative CANs based on epoxy resins Vitrimers [25–30]. Since 2011, interest in Vitrimers has increased, with many researchers introducing various dynamic covalent bonds and catalysts into epoxy resins to achieve Vitrimer like properties. Furthermore, many studies have explored the combination of different dynamic covalent chemistries within a single adaptable network, synthesizing a CAN with tuneable mechanical properties by changing the content of the incorporated reactions [31]. Taking this concept even further, some adaptable networks also include non-covalent reversible bonds such as hydrogen bonds [32], combining the benefits of supramolecular and reversible covalent chemistry within a single network.

The flow behavior of Vitrimers at elevated temperatures originates from the ability of covalent adaptable networks to reorganize their topology. This rearrangement occurs when sufficient energy is provided to the material, allowing both the physical interactions- the entanglements- between molecular chains and the chemical interactions- the dynamic crosslinks- to be overcome. Consequently, vitrimers exhibit two characteristic transition temperatures [25–30]. The first is the glass transition temperature T_g that marks the onset of chain mobility. Like thermosets and thermoplastics, T_g represents the transition from a rigid, glassy

state to a rubbery solid. The second characteristic temperature is the topology freezing transition temperature T_v, which marks the point at which dynamic covalent crosslink bonds are activated, allowing for rapid bond exchange. Increasing the temperature of Vitrimer above T_V results in polymer flow and the material transitions from a viscoelastic solid to a viscoelastic liquid. The topology freezing transition temperature T_V is defined as the temperature where the viscosity of the material reaches the value of 10^{12} Pa s.

The glass transition temperature arises from the physical interactions between molecular chains and reflects the point where mobility of chains is activated. In contrast, the topology freezing temperature arises from chemical interactions and more specifically, from the dynamic covalent bond exchange of the network. As a result, the glass transition temperature and the topology freezing transition temperature occur due to different interactions between the molecular chains, and there is no correlation between them [26]. In most cases reported in the literature, T_g lies below T_V. As a result, at temperatures below the glass transition, the Vitrimer exists in a rigid, glassy state and behaves like a conventional thermoset. When the temperature increases between T_g and T_v, the material transitions from a rigid solid to a viscoelastic solid. In this temperature range, the dynamic bond exchanges remain inactive, and therefore the viscosity remains high. At temperatures above T_v, rapid bond exchange reactions are activated, enabling the network to flow. The rate of flow is influenced by the rate of bond exchange reactions, and the corresponding decrease in viscosity is governed by the kinetics of the reactions and follows the arrhenius equation:

$$K = \omega \exp\left(-\frac{E_{\mathrm{a}}}{RT}\right) \tag{1}$$

This empirical equation 1 has been applied to describe the temperature dependence of Vitrimer viscosity [26, 33, 34]. In this equation, term K is the rate constant of bond exchange reactions, ω is the pre-exponential factor corresponding to the natural frequency of the reactive group- typically around $10^8 - 10^9\ \mathrm{s}^{-1}$ for small molecules and E_a represents the energy barrier of bond exchange process. By modifying the equation 1, it is possible to plot K as a function of the inverse temperature (1/T), from which the activation energy E_a can be determined from the slope of the line. The effect of Catalyst loading on Vitrimers remains a subject of debate. Some studies suggest that catalyst loading does not alter the activation energy E_a of bond exchange reactions but increases the overall rate of bond exchanges by increasing the pre-exponential term (ω) [35]. On the other hand, other reports support that the value of T_v can be tuned in a controlled manner by changing the catalyst content, higher catalyst content leads to a reduction in the topology freezing transition temperature [36, 37].

Nevertheless, some studies have reported Vitrimers that exhibit low topology freezing transition temperatures, in certain cases even lower than glass transition temperatures [38, 39]. Under these conditions,

chain segment mobility is very limited, preventing bond exchange reactions from occurring. Increasing the temperature above T_g causes the viscosity to sharply decrease according to the Williams-Landel-Ferry (WLF) equation -similar to dissociative CANs- and at even higher temperatures the viscosity is governed again by the kinetics of reactions, following the Arrhenius behavior. At this point, it should be emphasized that although glass transition temperature and the topology freezing transition temperature are independent with no direct correlation, the synthesis of low-T_g polymers is prerequisite for developing low-T_v vitrimers [39]. While this may appear contradictory, the explanation lies in chain flexibility. A low T_g corresponds to increased number of possible conformations of the polymer, allowing reactive groups to encounter each other and thereby facilitating the crosslink exchange. Contrary, polymers with a high T_g exhibit restricted chain mobility. Under such conditions even if bond exchange reaction is possible, their occurrence is negligible.

From the preceding discussion, it can be concluded that T_v should not be viewed as a fixed thermodynamic threshold, but rather as a variable temperature range governed by the kinetics of bond exchange reaction. So far, the ability of Vitrimers to undergo topology rearrangement via bond exchanges has been associated with the temperature as external stimuli.This is the reason why some studies refer to Vitrimers as thermoreversible CANs, although this terminology can be limiting.

Molecular Simulations proposed that bond exchanges can relax stress during deformation and therefore delay fracture improving the network toughness [40]. Taken together, these findings [41–43] indicate an underlying connection between applied loading, mechanical stress, and bond-exchange reactions. Although the role of mechanochemistry in dynamic covalent chemistry and CANs is still emerging, reasonable hypotheses can be proposed regarding how external stress may facilitate bond-exchange processes in vitrimers and, in turn, shape their mechanical response.

Mechanical stresses imposed on a network can distort molecular structures and alter energy barrier of bond exchange reactions; this effect is described by the Bell model and related mechanochemical theories [44, 45]. The potential for accelerating the associative mechanism of Vitrimers depends strongly on the type of external loading. Hydrostatic compression, without a corresponding temperature increase, is likely to hinder these reactions because it reduces free volume and segmental mobility, effectively raising the glass transition temperature [46], which as discussed earlier is critical for the kinetics of the dynamic reactions. On the other hand, shear or unconfined compression can introduce anisotropic deformation, creating regions of enhanced mobility within the network that reduces the activation energy according to the Bell model and the activation volume concept. Consequently, the effective topology freezing transition temperature may vary under different loading conditions. This reinforces the view that T_v should be considered as an operational parameter rather than an intrinsic static fundamental transition temperature of Vitrimers. The interplay

between stress and the kinetics of bond exchange becomes particularly relevant in practical applications of Vitrimers, which will be discussed in the following paragraphs.

The associative bond exchange mechanism of Vitrimer imparts key properties such as weldability, reprocessability or self-healing which can be exploited across a range of applications. One of the first major areas in which vitrimers are being actively investigated is recycling. Vitrimers offer the potential to replace conventional thermosets, such as epoxy, by enabling closed loop material recovery without significant loss of performance. Over the past decades, conventional thermosets have been extensively used as matrices for fiber reinforced composites owing to their low production cost and high specific properties, particularly in applications such as aircraft, wind turbine blades, and automotive structures [47]. The integration of these lightweight composites into civil transportation aircrafts was aligned with broader sustainability goals, as reducing structural weight directly lowers fuel consumption, contributing to 14 – 15% annual reduction in CO_2 emissions [48]. Despite these, the recycling of thermoset matrices remains a significant challenge. Thermosets including epoxies and polyurethanes account for approximately 12% of the global plastic production, corresponding to nearly 44 million tons annually. However, data from European Composite Industry Association indicate that only 25% of thermoset composite waste is accessible for recycling, and of that fraction, only 5% is currently recycled, with the vast majority ending up in landfills [49].

The permanent crosslink in conventional thermoset networks, while conferring desirable properties such as chemical stability and dimensional integrity, significantly hinders their recyclability. The dynamic nature of bond exchange mechanisms found in Vitrimers and other CANs offer a promising solution to this limitation, combining the mechanical performance of thermosets with the reprocessability and recyclability typically associated with the thermoplastics.The most widely adopted recycling process for Vitrimer materials, or resins containing a vitrimer fraction, is hot-pressing. The fractured specimens from mechanical testing are cut into smaller fragments or ground into powder. These fragments are then reprocessed into new plates by applying elevated temperature and pressure. From these reformed plates, new specimens can be constructed for further mechanical testing. This recycling process is by far the most reported in the literature and has been successfully employed across a wide range of materials containing various dynamic covalent chemistries [50–54].

Beyond their reprocessability and potential for thermoset recycling, the dynamic bonds in Vitrimers also offer self-healing capabilities. Many studies have incorporated Vitrimers and CANs into traditional epoxy matrix composites to evaluate their impact performance and to investigate their self-healing capabilities for impact-induced cracks [55–59].Conventional thermoset composites exhibit low interlaminar fracture toughness under impact loading, which often leads to delamination and loss of structural integrity [60].

This limitation has driven significant interest in developing composite materials that can be repaired. The results demonstrate that the modified vitrimer composites can recover a portion of their strength following delamination healing. The efficiency of this self-healing process depends on the fiber content, as the presence of fibers can hinder the underlying bond-exchange mechanisms.

B. CANs & Metamaterials

The incorporation of vitrimer materials into the epoxy matrices of composites has already been extensively investigated and another promising field where vitrimers could play a significant role is that of foams and mechanical metamaterials. Foams are cellular solids composed of randomly distributed pores throughout the bulk material [61]. Over the past decades, foams have been employed in a wide range of applications- from titanium foams used in implants to lightweight aluminum foams and sandwich structures utilized as aerospace components [62–66]. In contrast, mechanical metamaterials are artificially engineered structures that exhibit mechanical properties unattainable in natural materials, enabled by the deliberate design of their architected microstructures through periodic lattice arrangements [67, 68]. Based on their deformation mechanism under external loading, cellular solids -encompassing both foams and architected metamaterials- can be broadly categorized as bending dominated or stretching dominated structures. Conventional stochastic foams are predominantly bending dominated because their randomly oriented struts do not align axially with the load paths [69]. As a result, they exhibit relatively low-stiffness and strength to density ratios and are typically used in energy absorption and thermal insulation applications [70]. However, mechanical metamaterials can be designed so that the loads are carried primarily through axial stretching rather than bending, leading to significantly enhanced mechanical efficiency for load-bearing applications [71].

The distinction between these two deformation mechanisms is directly reflected in how the effective modulus scale with the relative density. Bending-dominated structures obey a quadratic scaling law [72–74]:

$$\frac{E}{E_s} \propto \left(\frac{\rho^*}{\rho_s}\right)^2$$

Thus as relative density decreases, the stiffness of a bending dominated cellular solid drops rapidly ,following a quadratic dependence. In contrast, stretching dominated structures exhibit a linear scaling relationship:

$$\frac{E}{E_s} \propto \left(\frac{\rho^*}{\rho_s}\right)$$

In this case, reductions in density cause much more modest losses in stiffness, making stretching-dominated materials significantly more efficient for lightweight load-bearing applications.

In the current literature, covalent adaptable networks (CANs) have been predominantly explored for the fabrication of 3D lattice materials using light-based additive manufacturing techniques such as stereolithography (SLA) and digital light processing (DLP), which rely on photoinitiated cross-linking of the resin [75–83]. Most studies focus on manufacturing-related parameters, particularly the printing resolution achieved in lattice materials, and highlight the advantages of 3D printing over traditional casting methods, which are typically time-consuming and struggle to produce samples with low porosity [77]. However, the healing capabilities enabled by bond-exchange reactions are typically demonstrated only in simplified geometries, such as dogbone specimens. To date, the mechanical characterization of CAN-based metamaterials and subsequent investigation of their crack-healing performance in complex lattice materials remain largely unexplored.

III. Design & Experimental Plan

A. Materials

The vitrimer used to manufacture the metamaterial structures was prepared by mixing Diglycidyl ether of Bisphenol A (DGEBA) and adipic acid in a 1:1 stoichiometric ratio, with the addition of 2.5 mol% of the catalyst TBD [84]. The precursors were cured in a hot press at 160°C and 10 MPa for 6 hours [85]. The curing process produced vitrimer plates with in-plane dimensions of 75 mm $\times$ 66 mm and a thickness of 3 mm, as shown in Figure 1.

B. Design of Metamaterials

The two topology designs evaluated in this study are shown in Figure 2. Both *meta1* and *meta2* consist of 3×3 unit cells with a strut thickness of 2 mm, and additional material is included at the ends to provide sufficient gripping length for mechanical testing. To allow a direct comparison of the mechanical performance and healing efficiency of the two topologies, the specimens were designed to have a similar relative density.

The calculations used to determine the relative densities of the metamaterial specimens are provided below:

The outer area of the metamaterial design is calculated as

$$A = 32 \text{ mm} \times 32 \text{ mm} = 1024 \text{ mm}^2.$$

The effective density of the metamaterial is defined by

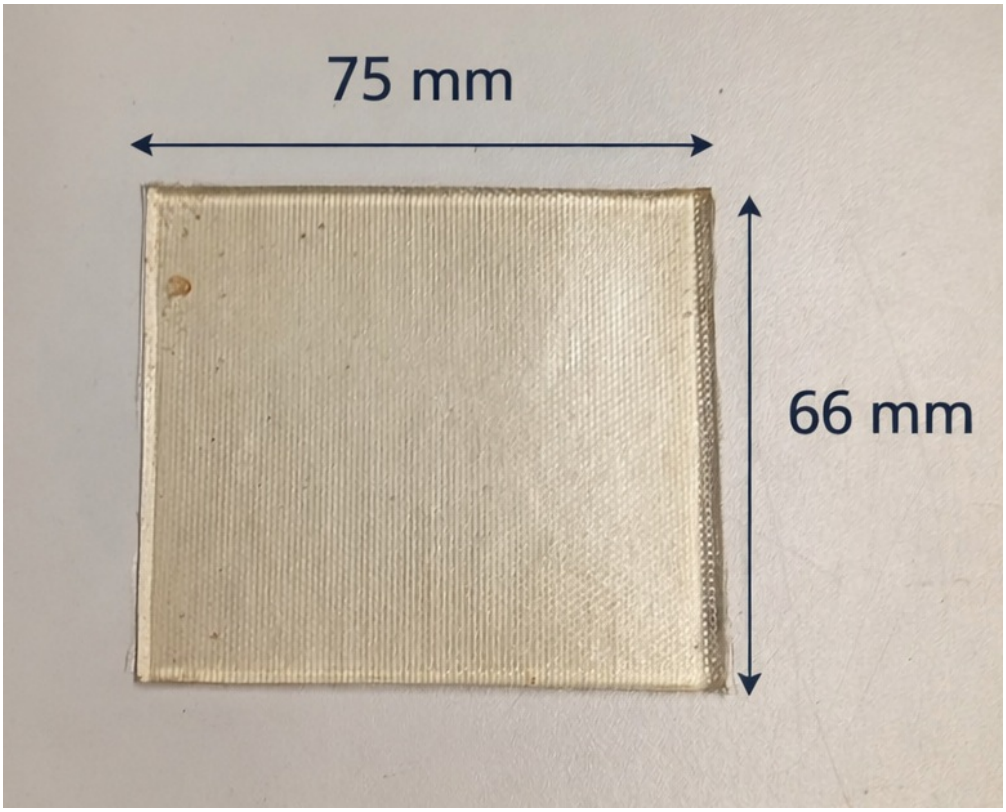

Figure 1. Measured dimensions of the fabricated vitrimer plates.

$$\rho^* = \frac{m^*}{V} = \frac{\rho_s A^* t}{At} = \rho_s \frac{A^*}{A},$$

where A^* denotes the solid area bearing load, A is the outer area, t is the thickness of the specimen, and ρ_s is the density of the solid material.

The relative density is therefore obtained as

$$\frac{\rho^*}{\rho_s} = \frac{A^*}{A} = \frac{445}{1024} \approx 0.43$$

A relative density of 43% lies at the upper end of the range typically used for cellular solids. Most cellular materials exhibit relative densities below 0.35, while many foams can reach extremely low values, even down to 0.003 [74]. This comparatively dense metamaterial design, together with the limited number of unit cells, was selected due to manufacturing constraints associated with the cutting resolution, as discussed in the following section.

By applying the Maxwell criterion, the dominant deformation mechanism of the two specimens can be identified. The criterion is given by

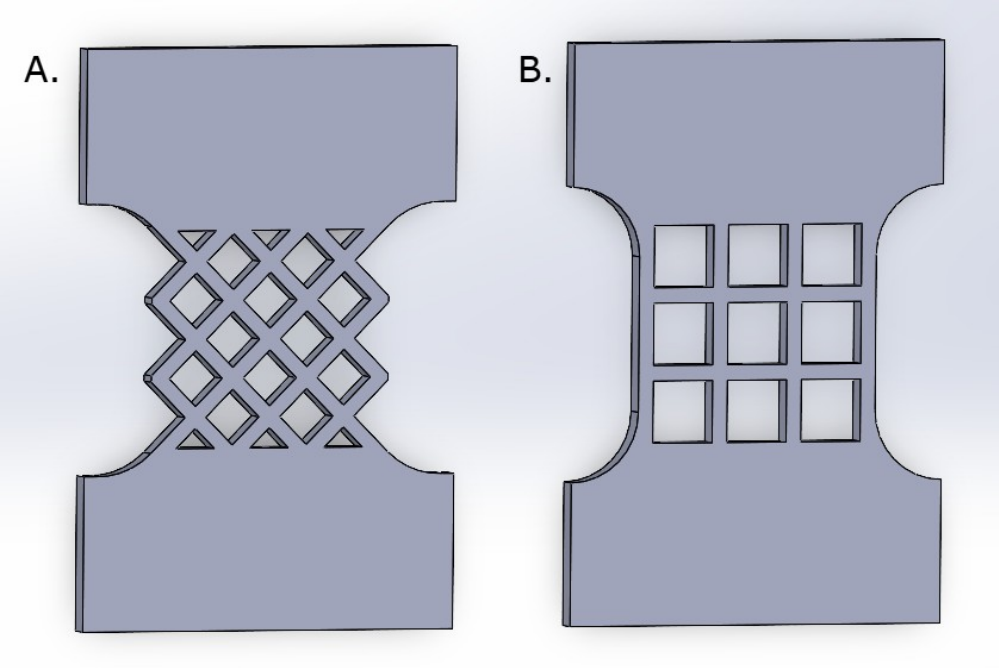

Figure 2. Topology designs of the two specimens. Specimen A is referred to as *meta1*, and specimen B as *meta2*.

$$M = b - 2j + 3,$$

where b and j denote the number of struts and nodes in the unit cell, respectively [70, 71, 86]. For *meta1* and *meta2*, the Maxwell index is negative (–3 and –1, respectively), indicating that both unit cells are bending-dominated. Although both metamaterial designs exhibit bending-dominated scaling, their effective stiffness diverge because their topological arrangement interacts differently with the externally applied stress state, despite having similar relative densities. This will be confirmed experimentally, but it is intuitive that a larger fraction of the total strain energy is expected to be stored in axial deformation for *meta2* than for *meta1*, since more of its struts align with the applied load, whereas the oblique members of *meta1* promote bending dominated deformation. Finally, it must be emphasized that the added material forming the gripping regions alters the deformation behavior of the lattices. This effect is more evident in *meta1* where the extra material effectively acts as an extra load bearing member within the unit cell. As a result, the imposed boundary conditions shift the lattice response toward a more stretching dominated mode.

C. Manufacturing of Metamaterials

For manufacturing the specimens, waterjet cutting was selected over laser cutting to avoid Vitrimer oxidation, which could compromise its healing efficiency. Because adipic acid Vitrimer is not commercially available, machining it proved challenging-particularly for the *meta1* geometry. Although producing individual struts of 2-3 mm thickness is feasible with waterjet cutting, the small triangular features in *meta1* created high local stress concentrations from the waterjet stream, leading to numerous manufacturing defects in the specimen. As shown in Figure 3, after iterating on and optimizing the waterjet-cutting parameters, the dogbone samples and *meta2* specimens were successfully produced without any cracks or defects. In contrast, the *meta1* specimens exhibit localized damage accumulation near the small triangular cuts.

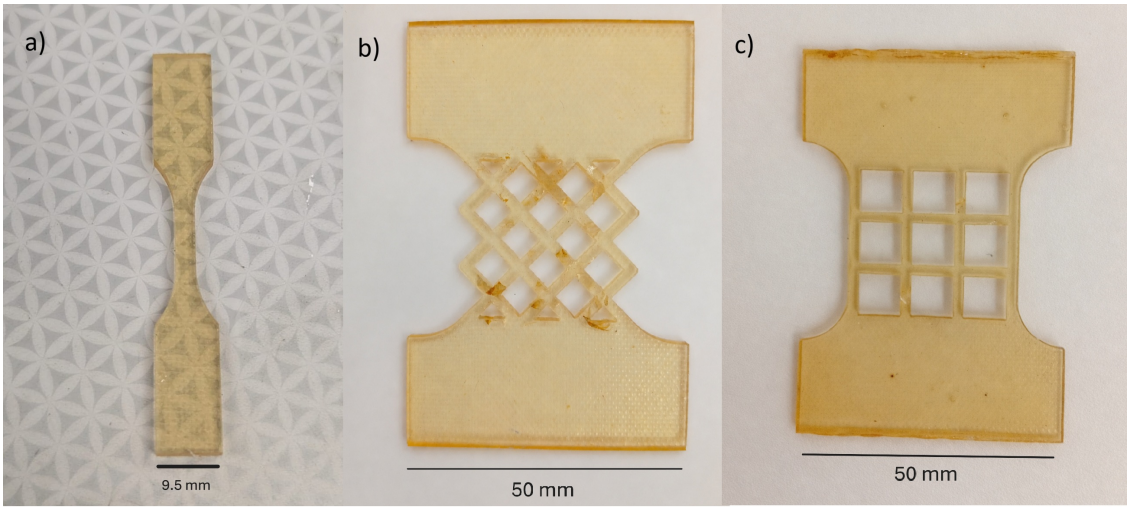

Figure 3. a) Waterjet-cut Adipic Acid Vitrimer dogbone specimen with gauge thickness of 3 mm b) Waterjet-Cut Meta1 specimen c) Waterjet-cut Meta2 specimen.

Figure 4 shows optical microscopy images of manufacturing defects. Numerous cracks are visible, distinguishable by the contrast arising from the different diffraction of the light on the fractured planes, which propagate across the entire unit cell. Several semi-spherical fractured surfaces are also observed caused by the abrasives in the waterjet stream. Although these defects introduce significant variability in the mechanical performance of the *meta1* specimens, they can be mitigated through the Vitrimer's bond exchange driven healing mechanism.

D. Mechanical testing

To establish fatigue-testing parameters and determine the appropriate mechanical testing setup, preliminary simulations were conducted alongside dummy tests on PVC and PTFE specimens with the same geometry. Figure 5 shows the first principal stress distribution for both specimens.

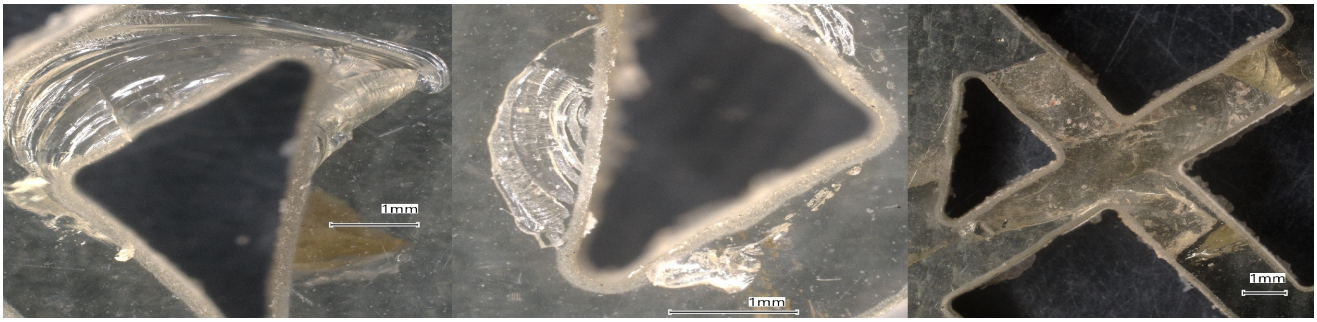

Figure 4. Manufacturing defects in the Meta1 specimen induced by waterjet cutting.

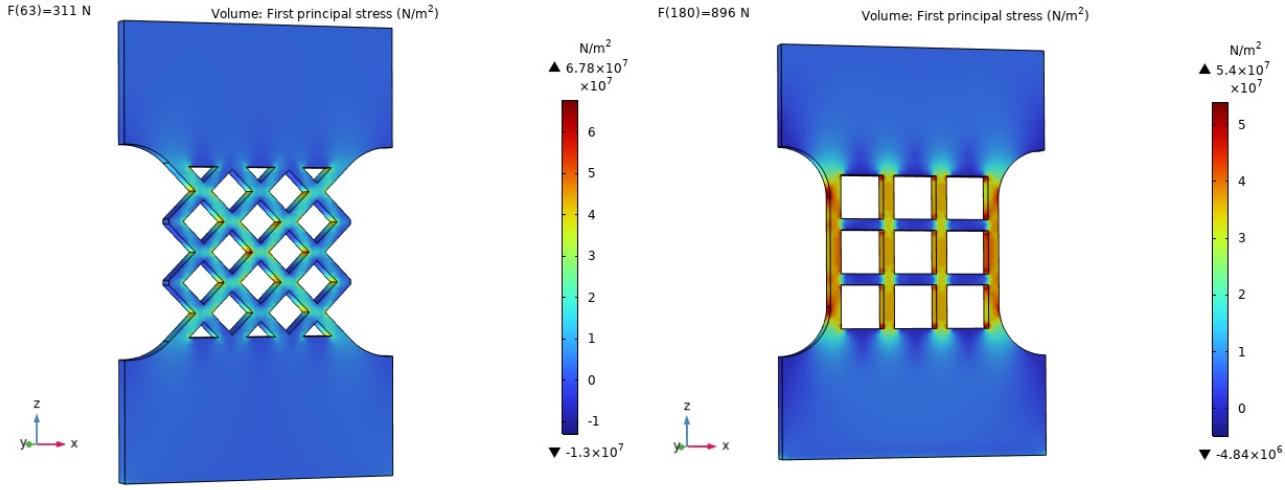

Figure 5. Finite-element simulations illustrating the mechanical response of the structures and the corresponding load paths.

In *meta1*, the primary tensile load path is concentrated along a subset of struts that form an "X"-shaped network connecting the gripping regions. The remaining struts mainly provide structural support, with some carrying compressive stresses that help stabilize the deformation. Although the structure is subjected to global uniaxial tension, its internal stress state becomes multiaxial due to the lattice geometry. This can be intuitively understood by considering the deformation of the diamond-shaped cells. When the structure is pulled vertically, the top and bottom nodes move apart while the lateral nodes displace sideways, resulting in a distortion of the cell. The distortion becomes evident during the testing of a *meta1* specimen fabricated from ductile base material, allowing sufficient plastic deformation for node rotation and structural rearrangement, as illustrated in Figure 6. This behavior introduces shear components into the internal stress state. The structure internally develops a stress state equivalent to combined tension and shear. Despite the presence of these clearly defined tensile paths, the struts involved are not primarily loaded in pure axial tension. Instead, due to the low rotational stiffness of the joints, significant node rotations occur, inducing bending in the struts. As a

result, the overall deformation mechanism of the structure remains bending-dominated, which is energetically more favorable than axial stretching for this topology.

In *meta2*, a larger number of struts are aligned with the loading direction, resulting in primary tensile load paths that are concentrated within these vertical members, as well as the node junctions. The engagement of multiple load-bearing struts oriented along the loading axis leads to a higher effective stiffness compared to *meta1*. To better understand the deformation, a single square unit cell can be considered. Under vertical tension, the upper and lower nodes move apart, causing the vertical struts to undergo a combination of axial stretching and bending due to node rotations. The horizontal struts, being perpendicular to the loading direction, primarily deform through bending and act as connectors that accommodate and transmit rotational motion between nodes. Although the vertical members experience axial deformation, their response is not purely axial. The stress distribution across their cross-section is non-uniform, and rotations at their ends introduce bending moments. Consequently, despite the presence of more direct load paths along the loading direction and an increased axial contribution, the overall deformation mechanism of the structure remains bending-dominated, albeit to a lesser extent than in *meta1*.

The two specimens were mechanically tested under low cycle fatigue. A 500 N load cell was employed, with *Meta2* subjected to a maximum stress $\sigma_{\max} = 1$ MPa and *Meta1* to $\sigma_{\max} = 333$ kPa. The minimum stress $\sigma_{\min}$ for both specimens was set to zero, which means that the stress ratio (R) of both low cycle fatigue scenarios was also zero. Practically, the fatigue tests subjected the specimens to tensile cyclic loading. A slow crosshead speed of 0.5 mm/min was selected, corresponding to a global strain rate of approximately $2 \times 10^{-4}\,\mathrm{s}^{-1}$. This value represents the strain rate of the overall structure, in lattices and cellular structures, local strain rates can be higher, particularly in regions that rotate, such as nodes. Despite this local heterogeneity, the loading remains fully quasistatic, ensuring that dynamic effects of the Vitrimer do not influence the structural response.

E. Reversing fatigue

Healing in the adipic acid Vitrimer requires activation of the underlying bond exchange reactions. This is achieved by elevating the temperature to near the topology freezing transition temperature, $T_v = 184$ °C, and by ensuring that the opposing crack surfaces are pressed into contact, allowing exchange reactions to occur across the interface. However, prolonged exposure to high temperature can lead to Vitrimer oxidation, as shown in Figure A1 in the Appendix. For this reason, a combination of moderate temperature and increased pressure is employed to promote healing while preventing thermal degradation.

Ideally, uniform healing of the numerous microcracks in the metamaterial specimens would be achieved

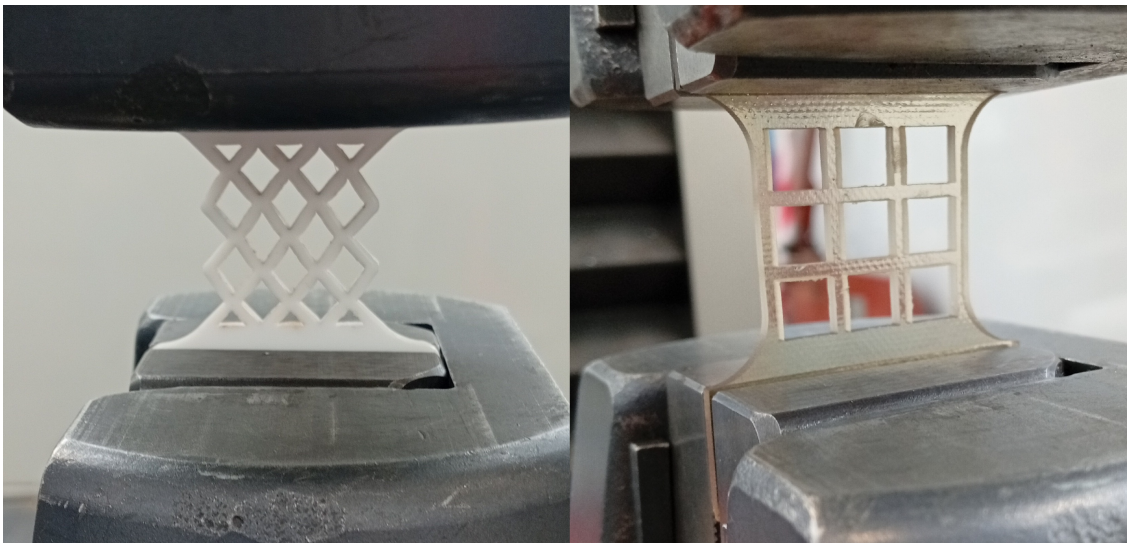

Figure 6. Distortion of the PTFE Meta1 unit cells and crack formation in the Vitrimer Meta2 specimen during cyclic loading.

by applying hydrostatic pressure. In practice, however, a mold and heat press setup was employed which imposes plane strain oedometric compression state. A vertical load is applied while lateral deformation is constrained, generating a triaxial but non-hydrostatic compressive stress field. Two mold designs were developed for this purpose, as shown in Figure 7.

Vitrimers adhere strongly to metal alloys, particularly when subjected to elevated temperatures and pressure. To prevent this, a common approach is to place a thin PTFE sheet (typically 0.10-0.30 mm) between the metal mold and the Vitrimer specimen. While effective for simple geometries such as plates or dogbones, this approach becomes unreliable for complex cellular architectures, where the PTFE sheet tends to tear. Consequently, a full PTFE block was adopted as mold material. The first mold design, presented in Figure 7a, consists of a CNC-machined PTFE block positioned within a hand-milled aluminum support frame. This mold design was suitable for only a single healing cycle, as the PTFE block shrank after removal from the heat press, resulting in a loss of dimensional integrity. To address this issue, a second design was implemented in which the CNC-machined PTFE block was mechanically fastened to the aluminium plate, as shown in Figure 7b.

IV. Results

As discussed in the simulations and in the analysis of the mechanical response of the two specimens, *meta2* experimentally exhibits a stiffness higher than *meta1*. Furthermore, as shown in Figure 8a, improving

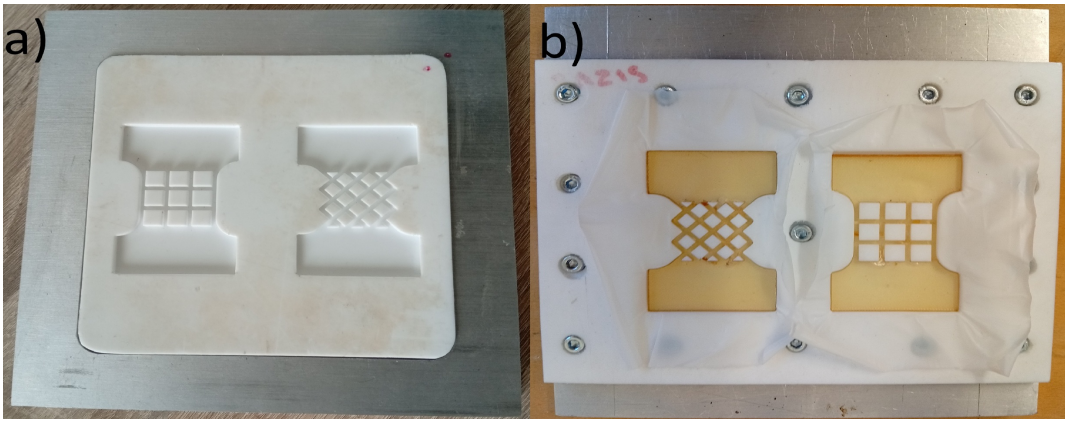

Figure 7. The two molds employed to facilitate crack healing in the specimens.

the waterjet-cutting parameters reduced the number of cracks in *meta1*, which was confirmed by mechanical testing through an increase in stiffness. In contrast, the stiffness variation in *meta2* is smaller because its specimens consistently exhibited good manufacturing quality regardless of the waterjet parameters.

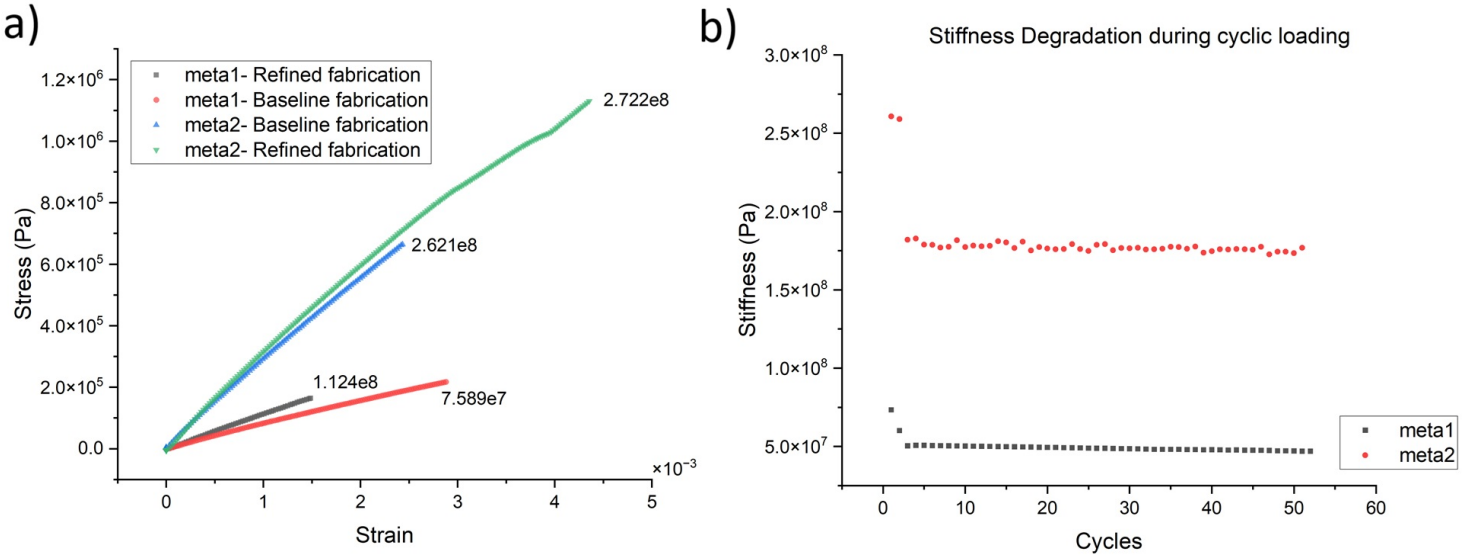

Figure 8. a) Effective stiffness of the specimens under different waterjet-cutting parameters. b) Stiffness degradation of both designs, with crack propagation occurring in the first cycles.

After experimental validation of the effective stiffness of the structures, both specimens were subjected to cyclic loading while monitoring stiffness degradation, as presented in Figure 8b. The *meta1* specimen exhibited two consecutive crack-propagation events during the first cycle, resulting in a shallow drop in its already low effective stiffness. In contrast, *meta2* showed a single crack propagation event that produced a substantial stiffness reduction of approximately 30% . Figure 9 illustrates the reason behind the large stiffness

loss, a crack that initially propagated through micropores eventually extended through the full strut thickness after cyclic loading, effectively removing the strut from load bearing. These optical microscopy images highlight the link between synthesis-induced defects in vitrimer, manufacturing conditions such as waterjet cutting that can trigger microcrack initiation at these defects, and the subsequent mechanical loading that drives crack propagation and failure. Additional optical microscopy images showing crack propagation are provided in Figure A2 in the Appendix.

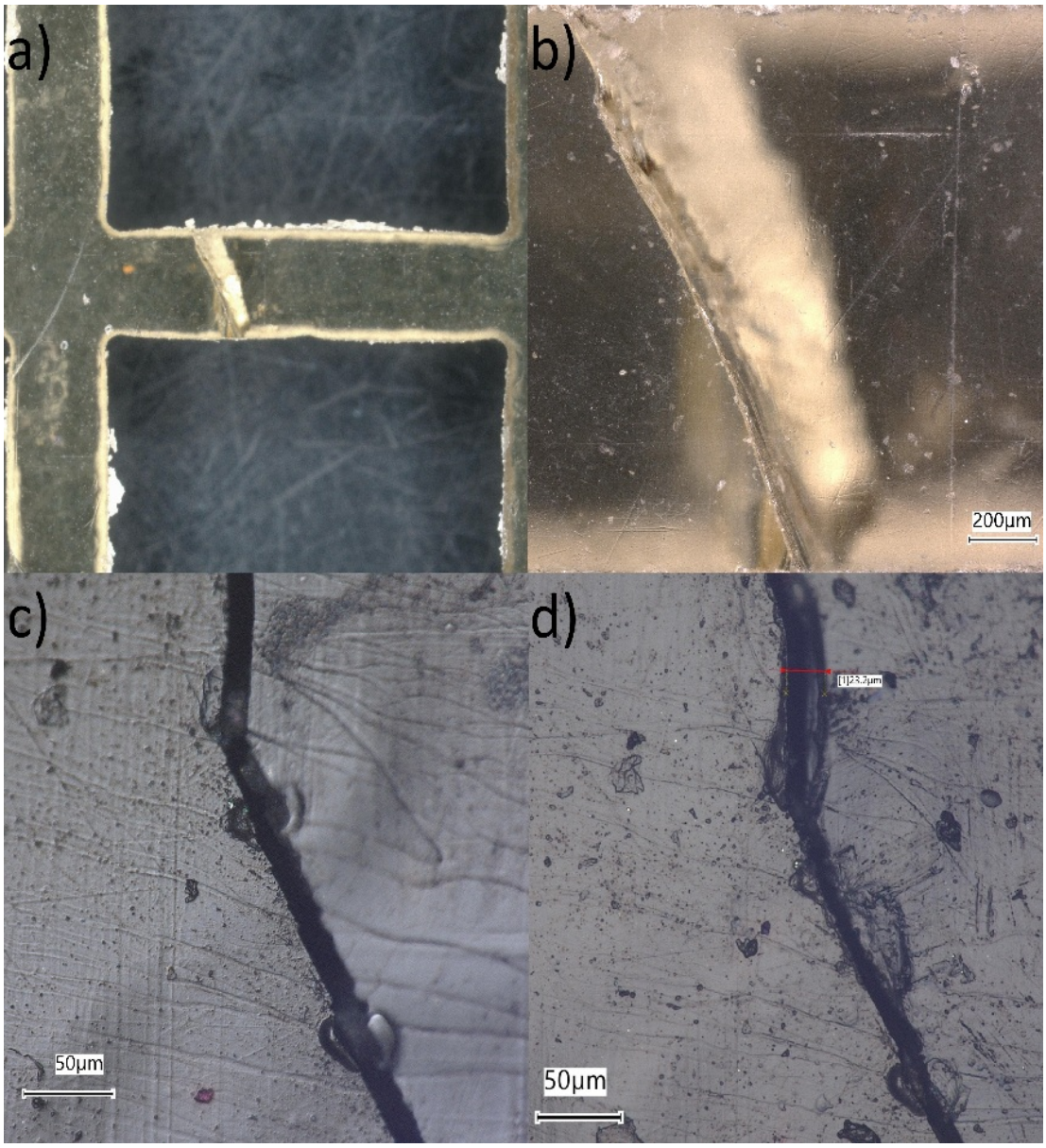

Figure 9. a) Crack propagation observed along a single strut. b) Crack fully propagating through the strut thickness, effectively removing it as a load bearing member. c) Early crack growth guided by micropores of approximately 25 μm. d) Enlargement of the crack opening following cyclic loading.

The healing parameters selected for both designs were 160 °C and 3 MPa for 7 hours. Several combinations of temperature and pressure were tested before these conditions were chosen as the most balanced for the setup that was used. As indicated in Figure 10, a higher temperature combined with low pressure results in inefficient healing and requires long durations, which may lead to Vitrimer degradation. Conversely, increasing the pressure improves crack-face contact and accelerates healing. However, applying high pressure can reduce specimen thickness, particularly when the mold lacks proper spacers. This is critical for precision components such as Vitrimer epoxy composites where excessive pressure can compromise dimensional integrity or even induce fibre waviness. Thus, although higher pressure enhances healing efficiency, it introduces other dentrimental effects. A balanced combination of temperature, pressure, and time must therefore be selected, specific to the Vitrimer chemistry used. Ideally, an experimental design matrix should be established for the Vitrimer system before attempting to heal components or specimens fabricated from it.

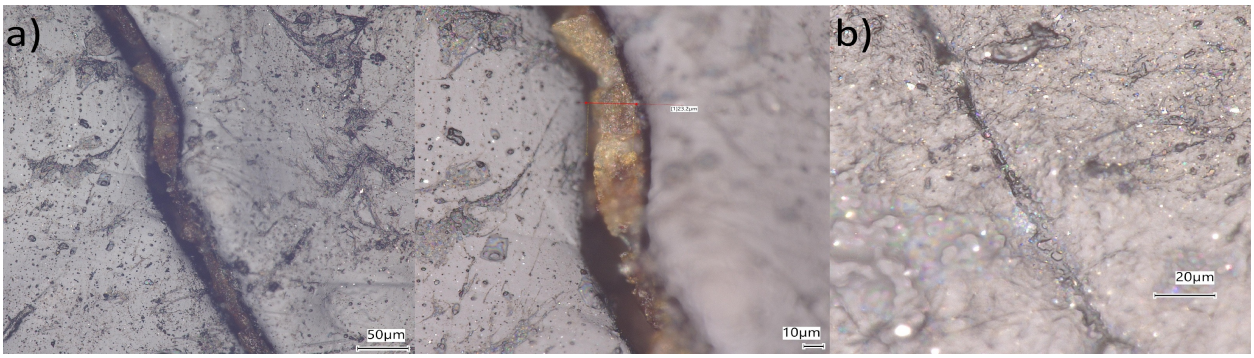

Figure 10. a) Two images showing inefficient crack healing at 180 °C under low pressure for 16 hours. b) Partial crack healing at 160 °C under 6 MPa after 4 hours.

After exploiting dynamic bond-exchange reactions to heal the cracks, the specimens were again subjected to cyclic loading to evaluate their recovered stiffness. As presented in Figure 11, the stiffness of the healed *meta1* appears significantly higher than in the pre-healing test. Although this initially seems counter-intuitive, it can be explained by the condition of the *meta1* specimens after waterjet cutting. Numerous manufacturing defects and cracks were present, and these were effectively healed. As a result, the recovered stiffness exceeds the original measured value. This interpretation is supported also by the optical microscopy observations presented in Figure A4. For the *meta2* specimen, stiffness was also recovered after the healing process, which was also validated with the optical microscopy observations presented in Figure A5, and the specimen maintained its stiffness without any crack propagation for approximately 45 cycles when a pronounced drop in stiffness occurred. This sharp decrease resulted from simultaneous crack propagation across multiple nodes, as shown in Figure A3, which severely compromised the load bearing capacity of the specimen.

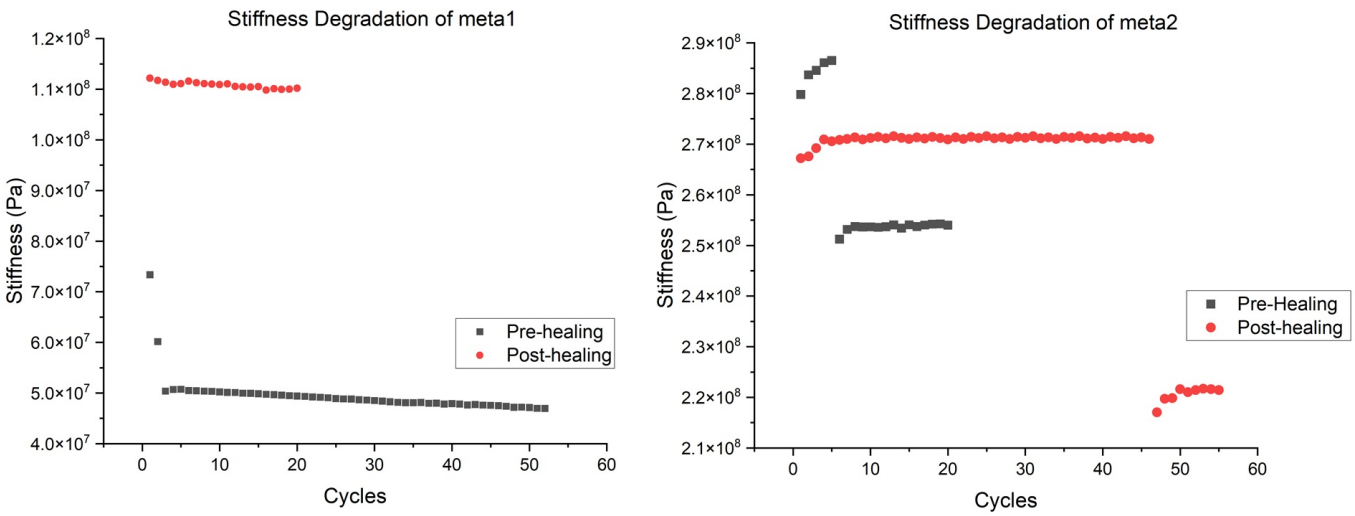

Figure 11. Graphs illustrating the recovered stiffness of the specimens after crack healing through Vitrimer bond-exchange reactions.

V. Discussion, Conclusions & Recommendation

Both specimen designs showed a pronounced sensitivity to manufacturing defects, with crack initiation during waterjet cutting occurring at micropores around 25 μm in size. These observations emphasize the importance of reducing porosity during Vitrimer synthesis and routinely assessing it through micro-CT imaging. Therefore, synthesis optimization should be supported by micro-CT analysis to establish processing conditions that minimize microvoid formation.

Regarding waterjet cutting for specimen preparation, Figure 4 illustrates that Vitrimer machining is particularly demanding for small and intricate features, such as those in the *meta1* architecture. Simpler geometries, including dogbone specimens, did not exhibit manufacturing cracks when examined under optical microscopy. For the adipic acid Vitrimer, optimal cuttability was obtained using polycarbonate cutting parameters, reduced speed and a supporting backplate. Future Vitrimer machining efforts should incorporate a finer abrasive, as the coarse abrasive currently employed is largely responsible for fractured surfaces and edge chipping.

Due to waterjet cutting limitations and restricted gripping configurations for mechanical testing, the 2D metamaterial specimens were fabricated with a 3x3 unit cell array. For future studies, increasing the number of unit cells would be preferable, as it would reduce boundary effects from the solid gripping regions and provide a more representative measurement of the lattice behavior.

Using PTFE molds in combinations with a heat press proved to be highly effective in healing cracks, even in complex geometries such as the 2D cellular specimens examined in this project. However, the engineering

and machining of the mold were challenging and had a substantial influence on the healing efficiency. Many Vitrimer studies report healing efficiencies based on dogbone specimens, yet this approach can be misleading as the measured efficiency is strongly dependent on how effectively the crack faces are brought into contact, which in turn is governed by mold design parameters such as tolerance. In the current work, improving the mold design directly enhanced the healing performance. Consequently, evaluating Vitrimer healing solely through dogbone samples may not accurately reflect the material's true healing capacity. Furthermore, the most rigorous strategy for optimizing Vitrimer healing is the development of an experimental design matrix to evaluate the influence of key factors -temperature, pressure, and time- on crack healing performance. This framework allows the identification of the optimal parameter set tailored to the Vitrimer chemistry under investigation. For example, in the adipic acid Vitrimer used in the present work, healing efficiency was maximized primarily by increasing the applied pressure.

Both *meta1* and *meta2* specimens were successfully healed, although the more compliant *meta1* design accumulated greater damage, making the healing process more challenging. In contrast, the more robust *meta2* architecture was easier to heal and more effectively recovered its stiffness. Although crack healing in 2D cellular solids is feasible using pressure-assisted crack closure, extending this approach to 3D cellular solids is not straightforward, as the applied pressure can distort their intricate geometries. For 3D architectures, healing may instead be achieved by self-healing polymer chemistries that require substantially lower pressure, or by incorporating conductivity enhancing particles at damage prone regions, such as nodes, to enable localized RF-induced heating. Overall, integrating self-healing polymers into metamaterial structures remains highly promising strategy for restoring their mechanical performance.

VI. Appendix

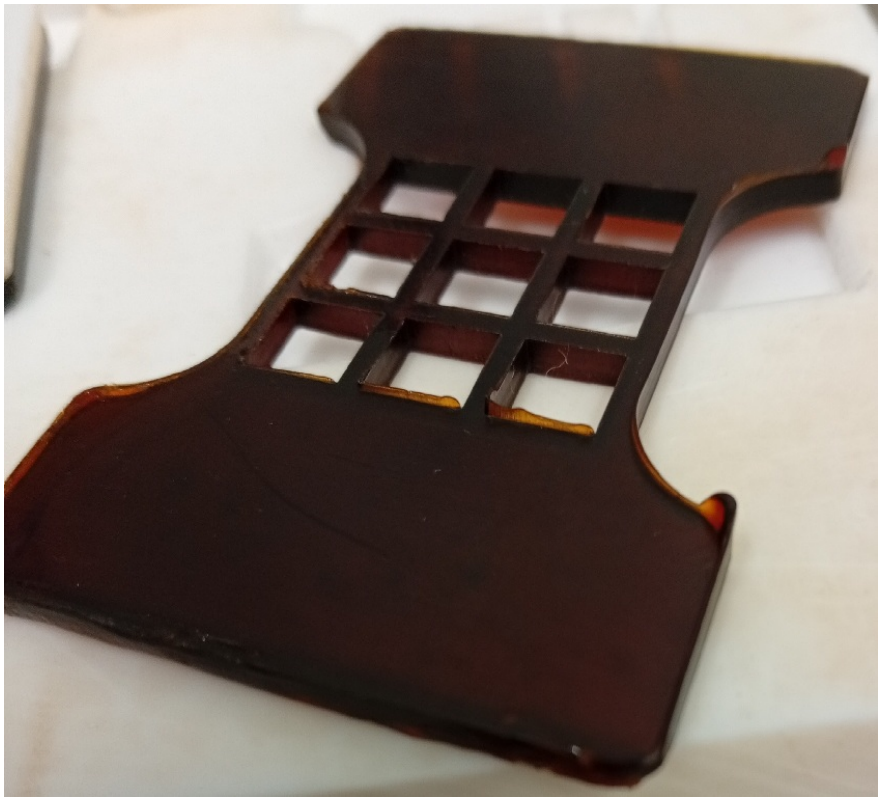

Figure A1. Oxidised Vitrimer Meta2 specimen resulting from prolonged exposure at 180 °C

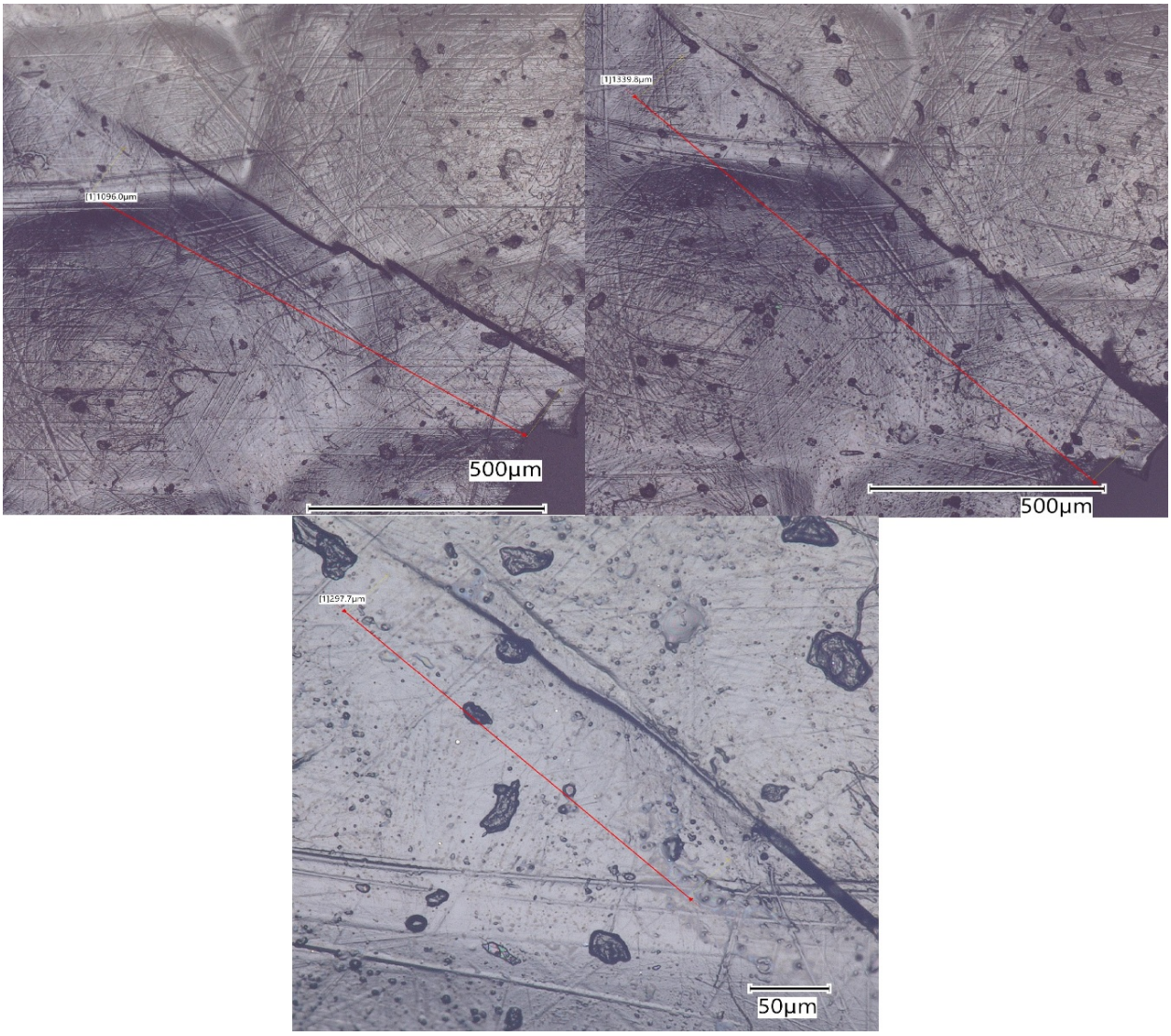

Figure A2. Evolution of crack propagation under cyclic loading

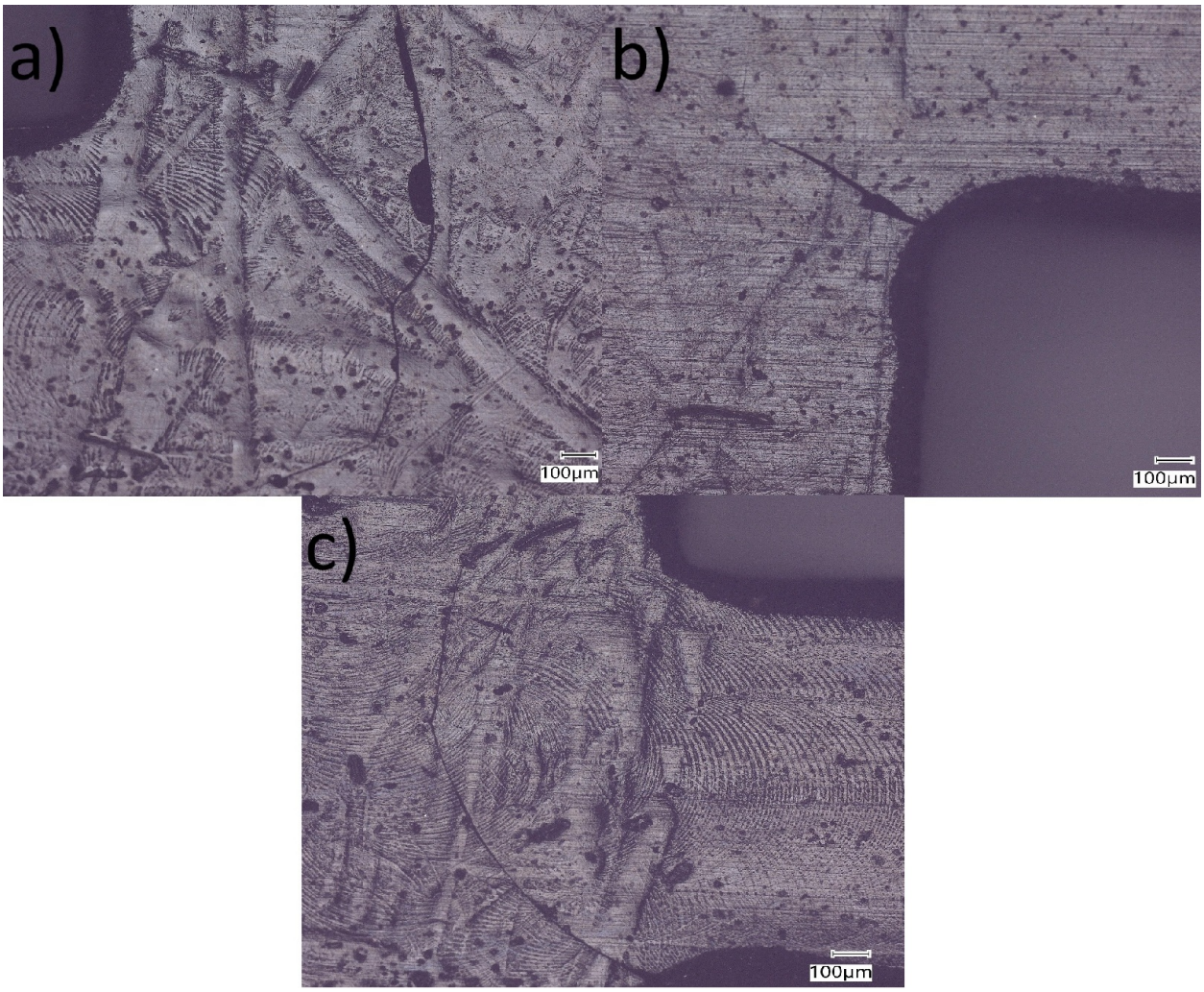

Figure A3. Simultaneous crack propagation at multiple nodes under cyclic loading.

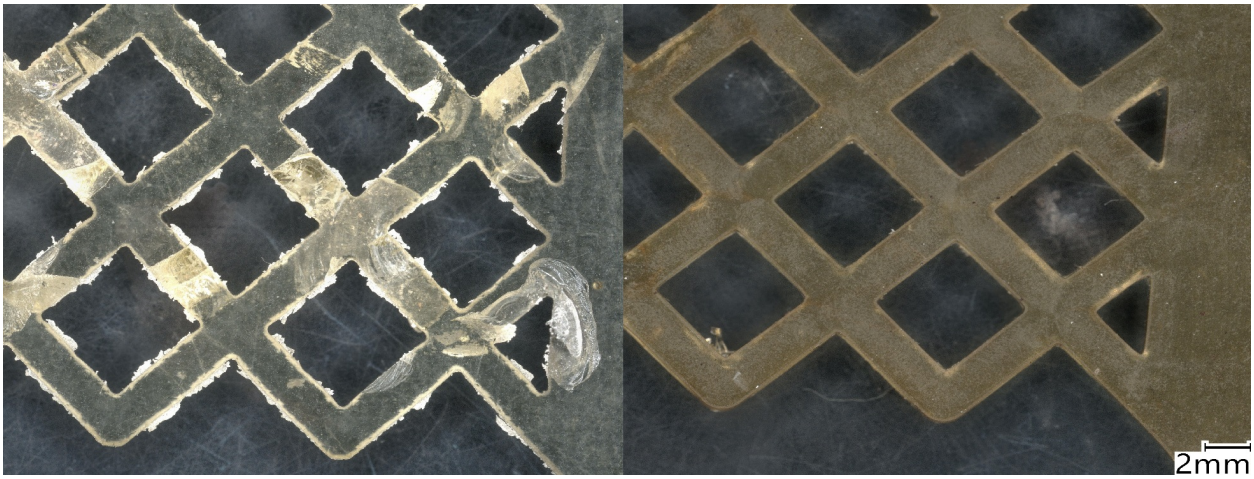

Figure A4. Optical microscopy images confirming crack healing in the meta1 specimen.

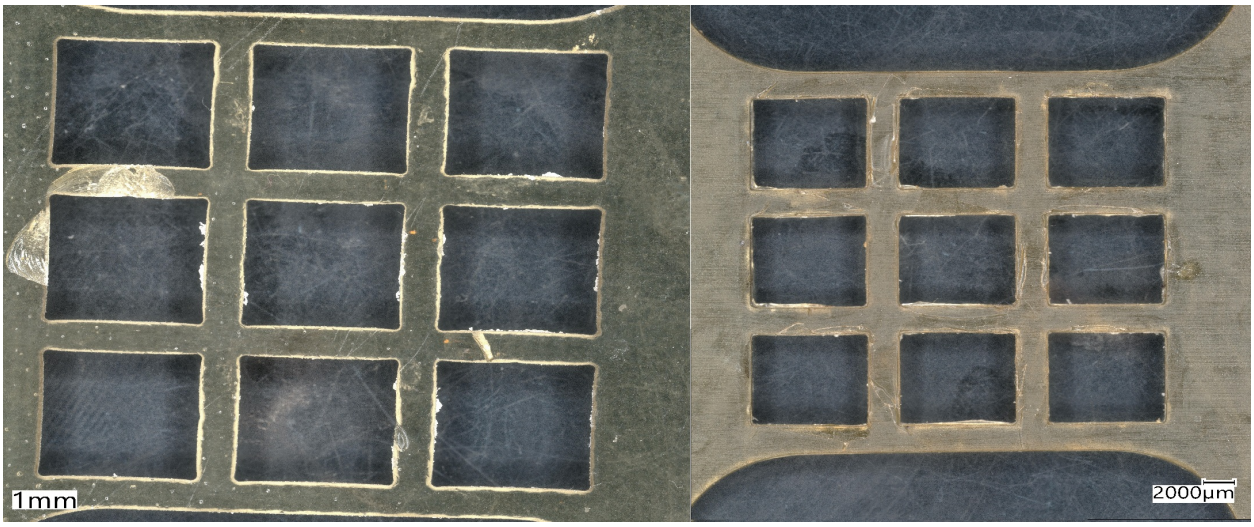

Figure A5. Optical microscopy images confirming crack healing in the meta2 specimen.

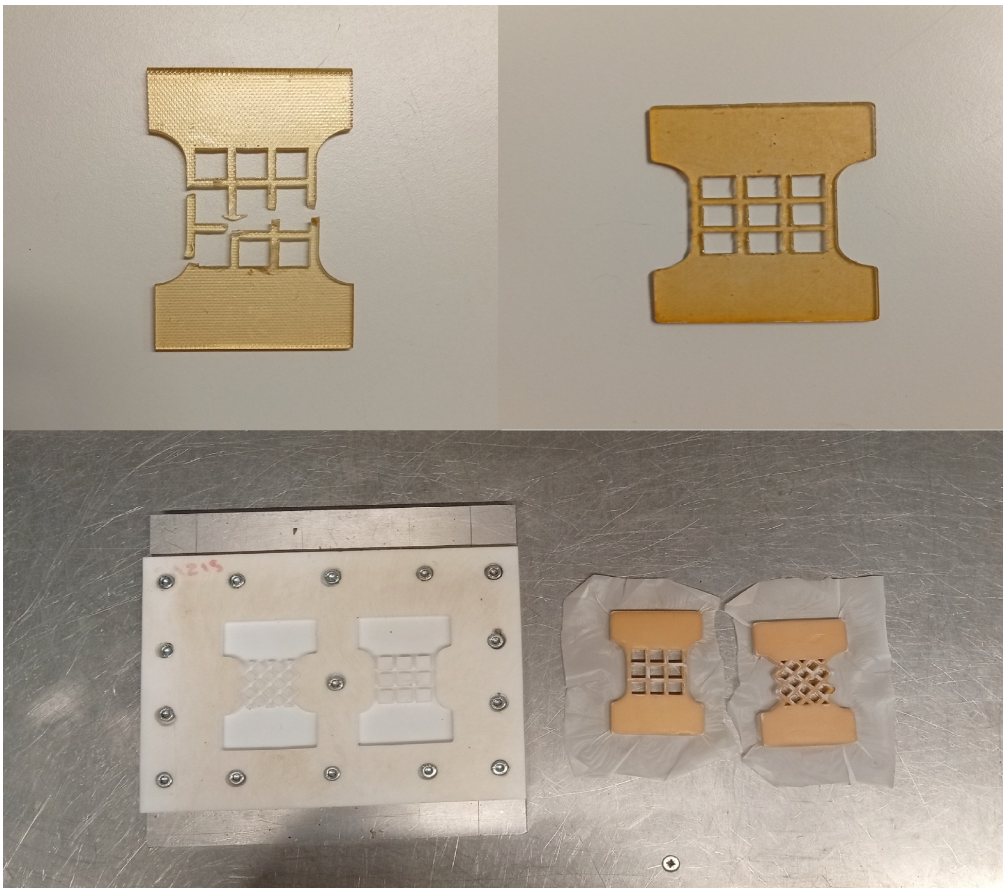

Figure A6. A fractured meta2 specimen, the same specimen after the healing process, and the mold with the healed specimens directly after heat pressing.

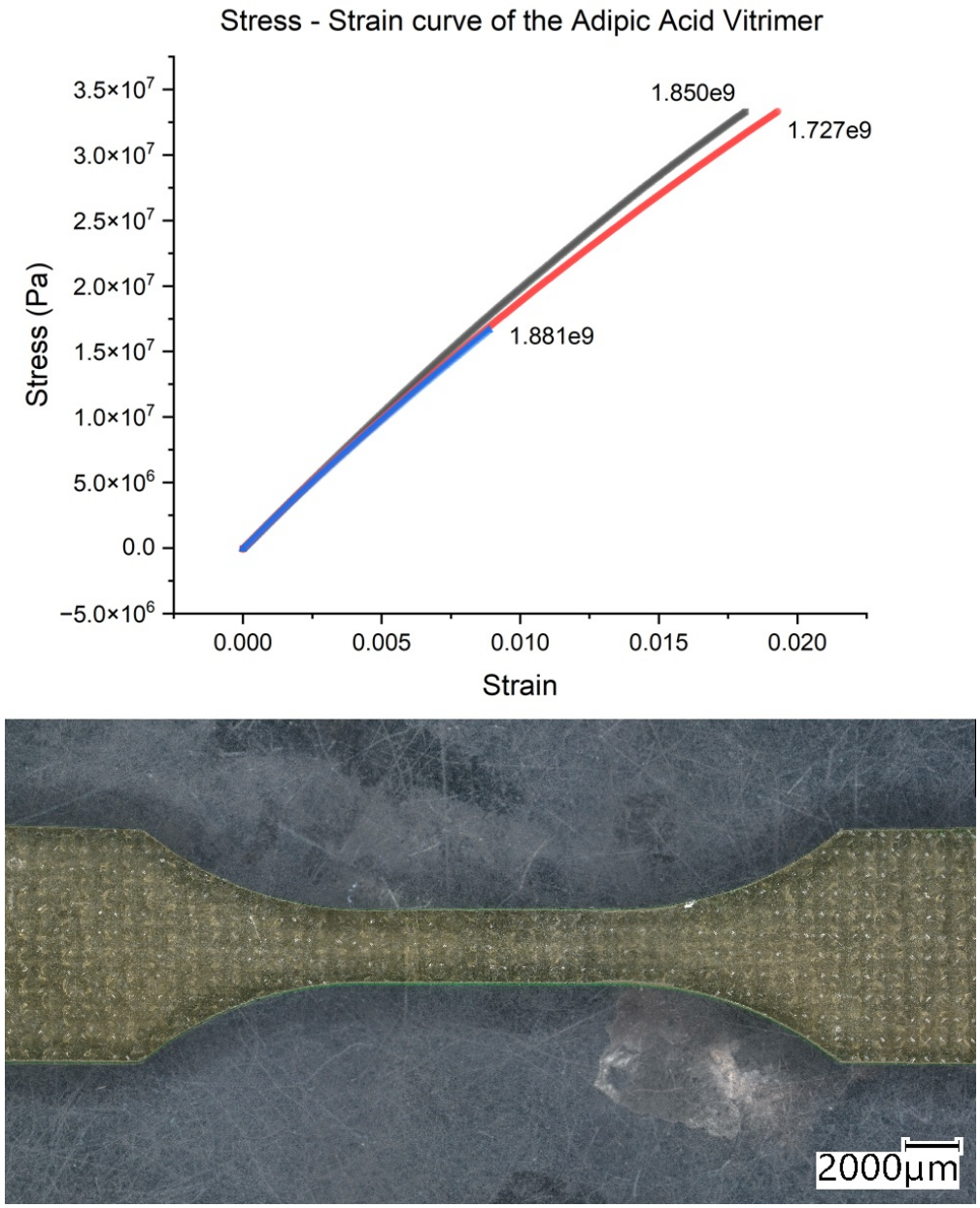

Figure A7. Dogbone specimens of the adipic-acid vitrimer were fabricated via waterjjet cutting and mechanically tested to evaluate the elastic response. The plotted stress-strain curve data represent only the initial linear regime (0.5- 1.5 % strain) which is relevant for determining the Young's modulus (1.8 GPa)

References

[1] Guimard, N. K., Oehlenschlaeger, K. K., Zhou, J., Hilf, S., Schmidt, F. G., and Barner-Kowollik, C., "Current Trends in the Field of Self-Healing Materials," *Macromolecular Chemistry and Physics*, Vol. 213, 2012, p. 131.

[2] Hager, M. D., Greil, P., Leyens, C., van der Zwaag, S., and Schubert, U. S., "Self-Healing Materials," *Advanced Materials*, Vol. 22, 2010, p. 5424.

[3] Kalista, S. J., Pflug, J. R., and Varley, R. J., "Effect of ionic content on ballistic self-healing in EMAA copolymers and ionomers," *The Royal Society of Chemistry*, 2013.

[4] Scheiner, M., Dickens, T. J., and Okoli, O., "Progress towards self-healing polymers for composite structural applications," *Polymer*, Vol. 83, 2015, p. 262.

[5] Zhou, Y., Li, L., Han, Z., Li, Q., He, J., and Wang, Q., "Self-Healing Polymers for Electronics and Energy Devices," *American Chemical Society*, 2022. Issue: Self-Healing in Chemical Systems.

[6] Hameed, N., Capricho, J. C., Salim, N., and Thomas, S., "Multifunctional Epoxy Resins: Self-Healing, Thermally and Electrically Conductive Resins," *Engineering Materials*, Springer, 2021, pp. 19–26.

[7] Greef, T. F. A. D., Smulders, M. M. J., Wolffs, M., Schenning, A. P. H. J., Sijbesma, R. P., and Meijer, E. W., "Supramolecular Polymerization," *Chemical Reviews*, Vol. 109, 2009, pp. 5689–5737.

[8] Dong, R., Zhou, Y., Huang, X., Zhu, X., Lu, Y., and Shen, J., "Functional Supramolecular Polymers for Biomedical Applications," *Advanced Materials*, Vol. 27, 2015, pp. 498–499.

[9] Cordier, P., Tournilhac, F., Ziakovic, C. S., and Leibler, L., "Self-Healing and Thermoreversible Rubber from Supramolecular Assembly," *Nature*, Vol. 451, 2008, p. 977.

[10] Aida, T., Meijer, E. W., and Stupp, S. I., "Functional Supramolecular Polymers," *Science*, Vol. 335, 2012, p. 814.

[11] Bergman, S. D., and Wudl, F., "Mendable Polymers," *Journal of Materials Chemistry*, Vol. 18, 2008, p. 42.

[12] Winne, J. M., Leibler, L., and Prez, F. E. D., "Dynamic Covalent Chemistry in Polymer Networks: A Mechanistic Perspective," *Polymer Chemistry*, Vol. 10, 2019, p. 6092.

[13] Bowman, C., Du Prez, F., and Kalow, J., "Introduction to chemistry for covalent adaptable networks," *Polymer Chemistry*, 2020.

[14] Tobolsky, A. V., "Stress Relaxation Studies of the Viscoelastic Properties of Polymers," *Journal of Applied Physics*, Vol. 27, 1956.

[15] McBride, M. K., Worell, B. T., Brown, T., Cox, L. M., Sowan, N., Wang, C., Podgorski, M., Martinez, A. M., and Bowman, C. N., "Enabling Applications of Covalent Adaptable Networks," *Annual Review of Chemical and Biomolecular Engineering*, 2019, pp. 176–178.

[16] Krishnakumar, B., Sanka, R. V. S. P., Binder, W. H., Parthasarathy, V., Rana, S., and Karak, N., "Vitrimers: Associative dynamic covalent adaptive networks in thermoset polymers," *Chemical Engineering Journal*, Vol. 385, 2020, p. 2.

[17] Khan, A., Ahmed, N., and Rabnawaz, M., "Covalent Adaptable Network and Self-Healing Materials: Current Trends and Future Prospects in Sustainability," *Polymers*, Vol. 12, 2020, pp. 1–3.

[18] Kloxin, C. J., Scott, T. F., Adzima, B. J., and Bowman, C. N., "Covalent Adaptable Networks (CANs): A Unique Paradigm in Cross-Linked Polymers," *Macromolecules*, Vol. 43, 2010, pp. 2643–2645.

[19] Kloxin, C. J., and Bowman, C. N., "Covalent Adaptable Networks: Smart, Reconfigurable and Responsive Network Systems," *Chemical Society Reviews*, Vol. 42, 2013, p. 7163.

[20] Bowman, C. N., and Kloxin, C. J., "Covalent Adaptable Networks: Reversible Bond Structures Incorporated in Polymer Networks," *Angewandte Chemie International Edition*, Vol. 51, 2012, p. 4271.

[21] Sheridan, R. J., and Bowman, C. N., "Understanding the Process of Healing of Thermoreversible Covalent Adaptable Networks," *Polymer Chemistry*, Vol. 4, 2012, p. 4974.

[22] Denissen, W., Winne, J. M., and Prez, F. E. D., "Vitrimers: Permanent Organic Networks with Glass-Like Fluidity," *Chemical Science*, 2015, p. 3.

[23] Williams, M. L., Landel, R. F., and Ferry, J. D., "The Temperature Dependence of Relaxation Mechanisms in Amorphous Polymers and Other Glass-Forming Liquids," *Journal of the American Chemical Society*, Vol. 77, 1955, pp. 3701–3702.

[24] Montarnal, D., Capelot, M., Tournilhac, F., and Leibler, L., "Silica-Like Malleable Materials from Permanent Organic Networks," *Science*, Vol. 334, 2011, pp. 965–966.

[25] Yang, Y., Wei, Y., and Ji, Y., *Functional and Sustainable Epoxy Vitrimers*, SpringerBriefs in Materials, Springer, 2022.

[26] Zheng, J., Png, Z. M., Ng, S. H., Tham, G. X., Ye, E., Goh, S. S., Loh, X. J., and Li, Z., "Vitrimers: Current Research Trends and Their Emerging Applications," *Materials Today*, Vol. 51, 2021, pp. 588–591.

[27] Zhang, H., Cui, J., Hu, G., and Zhang, B., "Recycling Strategies for Vitrimers," *International Journal of Smart and Nano Materials*, Vol. 13, 2022, pp. 368–371.

[28] Zee, N. J. V., and Nicolay, R., "Vitrimers: Permanently Crosslinked Polymers with Dynamic Network Topology," *Progress in Polymer Science*, Vol. 104, 2020, pp. 2–4.

[29] Guerre, M., Taplan, C., Winne, J. M., and Prez, F. E. D., "Vitrimers: Directing Chemical Reactivity to Control Material Properties," *Chemical Science*, Vol. 11, 2020, pp. 4856–4857.

[30] Yang, Y., Xu, Y., Ji, Y., and Wei, Y., "Functional Epoxy Vitrimers and Composites," *Progress in Materials Science*, Vol. 120, 2021, pp. 2–4.

[31] Delpierre, S., Willcoq, B., Manini, G., Lemaur, V., Goole, J., Gerbaux, P., Cornil, J., Dubois, P., and Raquez, J. M., "Simple Approach for a Self-Healable and Stiff Polymer Network from Iminoboronate-Based Boroxine Chemistry," *Chemistry of Materials*, Vol. 31, 2019, pp. 3736–3738.

[32] Liu, Y., Tang, Z., Wu, S., and Guo, B., "Integrating Sacrificial Bonds into Dynamic Covalent Networks toward Mechanical Robust and Malleable Elastomers," *ACS Macro Letters*, Vol. 8, 2019, p. 193.

[33] Meng, F., Saed, M. O., and Terentjev, E. M., "Rheology of Vitrimers," *Nature Communications*, Vol. 13, 2022, pp. 3–5.

[34] Meng, F., Pritchard, R. H., and Terentjev, E. M., "Stress Relaxation, Dynamics, and Plasticity of Transient Polymer Networks," *Macromolecules*, Vol. 49, 2016, pp. 2844–2845.

[35] Yang, Y., Zhang, S., Zhang, X., Gao, L., Wei, Y., and Ji, Y., "Detecting Topology Freezing Transition Temperature of Vitrimers by AIE Luminogens," *Nature Communications*, Vol. 10, 2019, p. 4.

[36] Capelot, M., Unterlass, M. M., Tournilhac, F., and Leibler, L., "Catalytic Control of the Vitrimer Glass Transition," *ACS Macro Letters*, Vol. 1, 2012, p. 790.

[37] Chen, Q., Li, Y., Yang, Y., Xu, Y., Qian, X., Wei, Y., and Ji, Y., "Durable Liquid-Crystalline Vitrimer Actuators," *Chemical Science*, Vol. 10, 2019, p. 3026.

[38] Krishnan, B. P., Saalwaechter, K., Adjedje, V. K. B., and Blinder, W. H., "Design, Synthesis and Characterization of Vitrimers with Low Topology Freezing Transition Temperature," *Polymers*, Vol. 14, 2022, pp. 5–7.

[39] He, C., Christensen, P. R., Seguin, T. J., Wood, B. M., Persson, K. A., Russell, T. P., and Helms, B. A., "Conformational Entropy as a Means to Control the Behavior of Poly(diketoenamine) Vitrimers In and Out of Equilibrium," *Angewandte Chemie International Edition*, Vol. 59, 2019, pp. 2–4.

[40] Pandya, H., and Khabaz, F., "Effect of dynamic bond concentration on the mechanical properties of Vitrimers," *ChemComm*, Vol. 60, 2024, pp. 10356–10357.

[41] Wang, Z., Wagner, R. J., Chen, T., Shah, S. P., Maiaru, M., and Silberstein, M. N., "Bond exchange reactions as a paradigm for mitigating residual stress in polymer matrix fiber composites," *International Journal of Solids and Structures*, Vol. 313, 2025, pp. 13–16.

[42] Fortman, D. J., Brutman, J. P., Cramer, C. J., Hillmyer, M. A., and Dichtel, W. R., "Mechanically Activated, Catalyst-Free Polyhydroxyurethane Vitrimers," *Journal of the American Chemical Society*, Vol. 137, 2015, pp. 14020–14021.

[43] Nishiie, N., Kawatani, R., Tezuka, S., Mizuma, M., Hayashi, M., and Kohsaka, Y., "Vitrimer-like elastomers with rapid stress-relaxation by high-speed carboxy exchange through conjugate substitution reaction," *Nature Communications*, Vol. 15, 2024, pp. 4–6.

[44] Boscoboinik, A., Olson, D., Adams, H., Hopper, N., and Tysoe, W. T., "Measuring and Modelling Mechanochemical Reaction Kinetics," *Chemical Communications*, Vol. 56, 2020, pp. 1–2.

[45] Bhuiyan, F. H., Li, Y., Kim, S. H., and Martini, A., "Shear-activation of mechanochemical reactions through molecular deformation," *Scientific Reports*, Vol. 14, 2024, pp. 1–2.

[46] Radcliffe, S. V., "Effects of Hydrostatic Pressure on the Deformation and Fracture of Polymers," *Deformation and Fracture of High Polymers*, Springer, 1973, pp. 191–198.

[47] Morici, E., and Dintcheva, N. T., "Recycling of Thermoset Materials and Thermoset-Based Composites: Challenge and Opportunity," *Polymers*, Vol. 14, 2022, pp. 2–3.

[48] Timmis, A. J., Hodzic, A., Koh, L., Bonner, M., Soutis, C., Schafer, A. W., and Dray, L., "Environmental impact assessment of aviation emission reduction through the implementation of composite materials," *International Journal of Life Cycle*, Vol. 20, 2015, pp. 239–243.

[49] European Composites Industry Association (EuCIA), "Reimagining end-of-use composites as a new resource," Brussels, 2025.

[50] de Luzuriaga, A. R., Martin, R., Markaide, N., Rekondo, A., Cabanero, G., Rodriguez, J., and Odriozola, I., "Epoxy Resin with Exchangeable Disulfide Crosslinks to Obtain Reprocessable, Repairable and Recyclable Fiber-Reinforced Thermoset Composites," *Materials Horizons*, Vol. 1, 2016, p. 4.

[51] Xu, C., Cui, R., Fu, L., and Lin, B., "Recyclable and heat-healable epoxidized natural rubber/bentonite composites," *Composites Science and Technology*, Vol. 167, 2018, p. 427.

[52] Imbernon, L., Oikonomou, E. K., Norvez, S., and Leibler, L., "Chemically crosslinked yet reprocessable epoxidized natural rubber via thermos-activated disulfide rearrangements," *Polymer Chemistry*, Vol. 6, 2015, p. 4277.

[53] Tang, Z., Liu, Y., Guo, B., and Zhang, L., "Malleable, Mechanically Strong, and Adaptive Elastomers Enabled by Interfacial Exchangeable Bonds," *Macromolecules*, Vol. 50, 2017, p. F.

[54] Zhang, Y., Yuan, L., Liang, G., and Gu, A., "Developing Reversible Self-healing and Malleable Epoxy Resins with High Performance and Fast Recycling through Building Crosslinked Network with New Disulfide-Containing Hardener," *Industrial & Engineering Chemistry Research*, Vol. 57, 2018, p. 20.

[55] Kostopoulos, V., Kotrotsos, A., Geitona, A., and Tsantzalis, S., "Low velocity impact response and post impact assessment of carbon fiber/epoxy composites modified with Diels-Alder based healing agent: A novel approach," *Composites Part A*, Vol. 140, 2021, p. 9.

[56] Ding, X., Chen, L., Xu, Y., Shi, X., Song, X., and Wang, Y., "Robust Epoxy Vitrimer with Simultaneous Ultrahigh Impact Property, Fire Safety, and Multipath Recyclability via Rigid-Flexible Imine Networks," *ACS Sustainable Chemistry & Engineering*, Vol. 11, 2023.

[57] Lin, Z., and Chen, P., "Experimental study on the high-velocity impact resistance of vitrimer-based carbon fiber composites," *Journal of Physics: Conference Series*, 2024, pp. 4–6.

[58] Sang, Z., Eoh, H., Xiao, K., Kurouski, D., Shan, W., Hyon, J., Sukhishvili, S. A., and Thomas, E. L., "Supersonic puncture-healable and impact resistant covalent adaptive networks," *Materials Today*, Vol. 83, 2025, pp. 48–50.

[59] Wang, C., Lei, G., Zhang, R., Zhou, X., Shen, J. Q., Luo, G., and Zhang, L., "Shear-Thickening Covalent Adaptive Networks for Bifunctional Impact-Protective and Post-Tunable Tactile Sensors," *Applied Materials & Interfaces*, Vol. 15, 2023.

[60] Saghafi, H., Brugo, T., Minak, G., and Zucchelli, A., "The effect of pre-stress on impact response of concave and convex composite laminates," *International Symposium on Dynamic Response and Failure of Composite Materials, Procedia Engineering*, Vol. 88, 2014, pp. 114–116.

[61] Al-Ketan, O., Rezgui, R., Rowshan, R., Du, H., Fang, N. X., and Al-Rub, R. K. A., "Microarchitected Stretching-Dominated Mechanical Metamaterials with Minimal Surface Topologies," *Advanced Engineering Materials*, 2023, pp. 2–3.

[62] Lefebvre, L., Banhart, J., and Dunand, D. C., "Porous Metals and Metallic Foams: Current Status and Recent Developments," *Advanced Engineering Materials*, 2008, pp. 780–784.

[63] Montillet, A., Comiti, J., and Legrand, J., "Application of metallic foams in electrochemical reactors of filter-press type. Part I: Flow characterization," *Journal of Applied Electrochemistry*, Vol. 23, 1993, pp. 1045–1050.

[64] Kausar, A., "Polyurethane Composite Foams in High-Performance Applications: A Review," *Polymer-Plastics Technology and Engineering*, 2017.

[65] Fukuda, A., Takemoto, M., Saito, T., Fujibayashi, S., Neo, M., Pattanayak, D. K., Matsushita, T., Sasaki, K., Nishida, N., Kokubo, T., and Nakamura, T., "Osteoinduction of porous Ti implants with a channel structure fabricated by selective laser melting," *Acta Biomaterialia*, 2011.

[66] Fukuda, A., Takemoto, M., Saito, T., Fujibayashi, S., Neo, M., Pattanayak, D. K., Matsushita, T., Sasaki, K., Nishida, N., Kokubo, T., and Nakamura, T., "Osteoinduction of porous Ti implants with a channel structure fabricated by selective laser melting," *Acta Biomaterialia*, 2011.

[67] Jiao, P., Mueller, J., Raney, J. R., Zheng, X., and Alavi, A. H., "Mechanical Metamaterials and Beyond," *Nature Communications*, Vol. 14, 2023, pp. 1–3.

[68] Zadpoor, A. A., "Mechanical meta-materials," *Materials Horizons*, Vol. 3, 2016, pp. 371–372.

[69] Al-Ketan, O., Rezgui, R., Rowshan, R., Du, H., Fang, N. X., and Al-Rub, R. K. A., "Microarchitected Stretching-Dominated Mechanical Metamaterials with Minimal Surface Topologies," *Advanced Engineering Materials*, 2018, pp. 1–2.

[70] Deshpande, V. S., Ashby, M. F., and Fleck, N. A., "Foam Topology: Bending versus Stretching Dominated

Architectures," *Acta Materialia*, Vol. 49, 2001, pp. 1038–1040.

[71] Deshpande, V. S., Fleck, N. A., and Ashby, M. F., "Effective properties of the octet-truss lattice material," *Journal of the Mechanics and Physics of Solids*, Vol. 49, 2001, pp. 1747–1750.

[72] Deng, B., Xu, R., Zhao, K., Lu, Y., Ganguli, S., and Cheng, G. J., "Composite bending-dominated hollow nanolattices: A stiff, cyclable mechanical metamaterial," *Materials Today*, Vol. 21, No. 5, 2018, pp. 469–472.

[73] Wallach, J. C., and Gibson, L. J., "Mechanical behavior of a three-dimensional truss material," *International Journal of Solids and Structures*, Vol. 38, 2001, pp. 7181–7186.

[74] Gibson, L. J., and Ashby, M. F., "The mechanics of foams: basic results," *Cellular Solids: Structure and Properties*, Cambridge University Press, 2014, Chaps. 1, 5, 2nd ed., pp. 175–190.

[75] Machado, T. O., Stubbs, C. J., Chiaradia, V., Alraddadi, M. A., Brandolese, A., Worch, J. C., and Dove, A. P., "A renewably sourced, circular photopolymer resin for additive manufacturing," *Nature*, 2024. doi: 10.1038/s41586-024-07399-9, URL https://doi.org/10.1038/s41586-024-07399-9.

[76] Zhu, G., Houck, H. A., Spiegel, C. A., Selhuber-Unkel, C., Hou, Y., and Blasco, E., "Introducing Dynamic Bonds in Light-based 3D Printing," *Advanced Functional Materials*, 2023. doi: 10.1002/adfm.202300456, URL https://doi.org/10.1002/adfm.202300456.

[77] Li, X., Yu, R., He, Y., Zhang, Y., Yang, X., Zhao, X., and Huang, W., "Self-Healing Polyurethane Elastomers Based on a Disulfide Bond by Digital Light Processing 3D Printing," *ACS Macro Letters*, Vol. 8, 2019, pp. 1511–1516. doi: 10.1021/acsmacrolett.9b00776, URL https://doi.org/10.1021/acsmacrolett.9b00776.

[78] Robinson, L. L., Self, J. L., Fusi, A. D., Bates, M. W., Read de Alaniz, J., Hawker, C. J., Bates, C. M., and Sample, C. S., "Chemical and Mechanical Tunability of 3D-Printed Dynamic Covalent Networks Based on Boronate Esters," *ACS Macro Letters*, Vol. 10, 2021, pp. 857–863. doi: 10.1021/acsmacrolett.1c00245, URL https://doi.org/10.1021/acsmacrolett.1c00245.

[79] Li, X., Yu, R., He, Y., Zhang, Y., Yang, X., Zhao, X., and Huang, W., "Four-dimensional printing of shape memory polyurethanes with high strength and recyclability based on Diels–Alder chemistry," *Polymer*, Vol. 200, 2020, p. 122532. doi: 10.1016/j.polymer.2020.122532, URL https://doi.org/10.1016/j.polymer.2020.122532.

[80] Zhang, B., Kowsari, K., Serjouei, A., Dunn, M. L., and Ge, Q., "Reprocessable thermosets for sustainable three-dimensional printing," *Nature Communications*, Vol. 9, 2018, pp. 1–8. doi: 10.1038/s41467-018-04292-8, URL https://doi.org/10.1038/s41467-018-04292-8.

[81] Durand-Silva, A., Cortés-Guzmán, K. P., Johnson, R. M., Perera, S. D., Diwakara, S. D., and Smaldone, R. A., "Balancing Self-Healing and Shape Stability in Dynamic Covalent Photoresins for Stereolithography 3D Printing," *ACS Macro Letters*, Vol. 10, 2021, pp. 486–491. doi: 10.1021/acsmacrolett.1c00041, URL https://doi.org/10.1021/acsmacrolett.1c00041.

[82] Yu, K., Xin, A., Du, H., Li, Y., and Wang, Q., "Additive manufacturing of self-healing elastomers," *NPG Asia Materials*, Vol. 11, 2019, p. 7. doi: 10.1038/s41427-019-0109-y, URL https://doi.org/10.1038/s41427-019-0109-y.

[83] Caprioli, M., Roppolo, I., Chiappone, A., Larush, L., Pirri, C. F., and Magdassi, S., "3D-printed self-healing hydrogels via Digital Light Processing," *Nature Communications*, Vol. 12, 2021, pp. 1–10. doi: 10.1038/s41467-021-22802-z, URL https://doi.org/10.1038/s41467-021-22802-z.

[84] Biswal, A. K., Gupta, S., Zhou, X., Lewis, T. K., Tang, J., and Vashisth, A., "Radio frequency (RF) enabled forming of vitrimers for moldless manufacturing," *Carbon*, Vol. 238, 2025, p. 2.

[85] Kamble, M., Vashisth, A., Yang, H., Pranompont, S., Picu, C. R., Wang, D., and Koratkar, N., "Reversing fatigue in carbon-fiber reinforced vitrimer composites," *Carbon*, Vol. 187, 2022, pp. 108–110.

[86] Fleck, N. A., Deshpande, V. S., and Ashby, M. F., "Micro-architectured materials: past, present and future," *Proceedings of the Royal Society A: Mathematical, Physical and Engineering Sciences*, Vol. 466, No. 2121, 2010, pp. 2502–2505. doi: 10.1098/rspa.2010.0215, URL https://doi.org/10.1098/rspa.2010.0215.